Journal of Marine Systems 187 (2018) 250–259

Contents lists available at ScienceDirect

Journal of Marine Systems

journal homepage: www.elsevier.com/locate/jmarsys

A method for correcting seal-borne oceanographic data and application to the estimation of regional sea ice thickness

Eamon K. Frazer[a,*], Pat J. Langhorne[a], Michael J.M. Williams[b], Kimberly T. Goetz[b], Daniel P. Costa[c]

[a] University of Otago, Department of Physics, PO Box 56, Dunedin 9016, New Zealand
[b] National Institute of Water and Atmospheric Research (NIWA), Private Bag 14901, Wellington 6021, New Zealand
[c] University of California, Department of Ecology & Evolutionary Biology, 100 Shaffer Road, Santa Cruz, CA 95060, United States of America

ARTICLE INFO

Keywords:
Antarctica
Ross Sea [75.5–78.0° S, 162–167° E]
CTD profilers
Sea ice
Ice thickness
Weddell seals
Salinity correction

ABSTRACT

The high-latitude oceans surrounding Antarctica are substantially undersampled compared to lower latitudes. Mammal based instruments such as Conductivity-Temperature-Depth Satellite Relay Data Loggers (CTD-SRDLs) present one possible solution. Unfortunately, these are subject to instrument-dependent offsets in absolute salinity. This study investigates a set of satellite-transmitted data collected by CTD-SRDLs mounted on Weddell seals (*Leptonychotes weddellii*) in the South-western Ross Sea in 2011. The uncorrected salinity offset between devices was found to be up to 1.4 g kg^{-1}, making the data unsuitable for some oceanographic studies without correction. Here, a correction method was developed that uses profiles from pairs of CTD-SRDLs that are considered to be co-located and to sample the same body of water if they occur within defined time and space windows. Using least squares, a best-fit solution to the matrix of offsets in co-located pairs was found that reduces salinity offsets between the CTD-SRDLs. These offsets are smaller than the original offsets by a factor of 10. A calibrated reference instrument, that was co-located with some of the devices, provided further improvement in the absolute accuracy of all the CTD-SRDLs. Using the corrected CTD-SRDL data we estimate the rejection of salt into the water column by sea ice formation, and derived the time evolution of sea ice thickness in the South-western Ross Sea. Our estimates of regional sea ice thickness are in agreement with direct sea ice thickness measurements taken over a limited area in November 2011, providing further affirmation of our method.

1. Introduction

There is significant evidence of Antarctic waters freshening and becoming warmer (e.g. Aoki et al., 2005; Levitus et al., 2000; Jacobs et al., 2002), with warming occurring at rates faster than the global mean (Gille, 2002). Nonetheless, oceanographic and sea ice thickness measurements at extreme latitudes are undersampled, especially in winter. This is partially because of the harsh conditions, but also because of the vast area that is encompassed. The ability to continuously observe and interpret the changes taking place in the Southern Ocean, and identify the mechanisms driving these changes, is a high priority for climate scientists and requires more observations at higher latitude, particularly in winter under sea ice (e.g. Meredith et al., 2016, 2013).

Remote sensing by satellite presents a possible solution to making observations, but only allows sea surface temperature (SST) to be measured when there is no significant ice cover. Further, the scarcity of in situ measurements of Antarctic sea ice thickness means that there is a need for improved temporal and spatial thickness data by satellite methods (e.g. Kurtz and Markus, 2012; Xie et al., 2013; Zwally et al., 2008). The estimation of remotely sensed sea ice thickness is based on the measurement of freeboard (elevation of the snow/ice upper surface above the ocean), in conjunction with snow depth and the densities of ice and snow (e.g. Zwally et al., 2008; Kurtz and Markus, 2012; Price et al., 2013). Given the heterogeneous and thinner state of Antarctic sea ice, primarily due to its more dynamic nature, and its highly variable snow distribution and morphology (e.g. Ozsoy-Cicek et al., 2013; Massom et al., 2001), the uncertainty in thickness estimates in the Southern Ocean is large in comparison with Arctic equivalents (Price et al., 2015).

Under-ice oceanographic information is available from platforms

* Corresponding author.
E-mail addresses: fraea318@student.otago.ac.nz (E.K. Frazer), pat.langhorne@otago.ac.nz (P.J. Langhorne), Mike.Williams@niwa.co.nz (M.J.M. Williams), Kim.Goetz@niwa.co.nz (K.T. Goetz), costa@ucsc.edu (D.P. Costa).

https://doi.org/10.1016/j.jmarsys.2018.08.002
Received 26 January 2018; Received in revised form 30 July 2018; Accepted 2 August 2018
Available online 09 August 2018
0924-7963/

such as Argo floats, which record salinity and temperature profiles. However, these cannot surface to transmit once ice cover becomes extensive, disabling them from providing location information if recovered (Pellichero et al., 2017), nor are they typically deployed on Antarctica's continental shelves. Ship-based measurements in contrast are reliable, but expensive and slow (Smith et al., 2014).

In comparison to other platforms, seal-borne instruments provide a significant advantage with their ability to collect oceanographic measurements in these harsh environments over large areas throughout the year even in high sea ice concentrations. Seals are able to find breaks in ice, permitting data transmission (Treasure et al., 2017). Satellite transmissions allow the collection of near real-time measurements over all seasons, often from data-sparse regions (Fedak, 2004), providing vertical oceanographic profiles of temperature and conductivity. This near real-time transmission is necessary to implement a fully continuous ocean monitoring system to study ocean structure over time (e.g. Charrassin et al., 2008; Costa et al., 2008; Meredith et al., 2011; Roquet et al., 2009, 2013).

The primary seal-borne oceanographic sensor in current use is the Conductivity-Temperature-Depth Satellite Relay Data Logger (CTD-SRDL), developed by the Sea Mammal Research Unit at the University of St Andrews (St Andrews Sea Mammal Research Unit, 2003). However, this instrument has an offset in salinity that occurs during deployment, which is related to the effect of the seal on the inductive field of the CTD-SRDL (Böhme et al., 2009). This offset is on the order of 10^{-1} g kg^{-1} (Böhme et al., 2009) and assumed to be constant in space and time, but varies between individual deployments (Durand and Reverdin, 2005). These data share a similar distribution, but are shifted along the salinity axis. Without correcting this offset, the ability to measure salinity with sufficient accuracy for many oceanographic applications is limited.

Post-processing methods already exist to correct these offsets (e.g. Böhme and Send, 2005; Roquet et al., 2011) but these typically rely upon either low interannual variability of water masses, historical observations or data from Argo floats for calibration. In shallower coastal oceans, such as the South-western Ross Sea, these options are not available. In lieu of these, we developed a simple method for making calibrations by comparing CTD-SRDL data to a high-quality reference device that operated simultaneously (spatially and temporally) with a subset of the CTD-SRDLs. We used a Sea-Bird Electronics SBE-41 (Sea-Bird Electronics, 2014) on an Ice-Tethered Profiler (ITP) as a reference device (Krishfield et al., 2008). In this study, not every CTD-SRDL was operating simultaneously with or near to the ITP. Therefore we developed an approach where we obtained a correction for the offset by cross-comparison of the CTD-SRDLs and the reference device simultaneously. We then applied this technique to our CTD-SRDL measurements obtained in the South-western Ross Sea during 2011. After correcting using this technique, we investigated changes in the oceanographic structure of the South-western Ross Sea over 9 months. We have demonstrated the utility of these derived regional changes in oceanographic structure over time by estimating the time evolution of sea ice thickness using the corrected data.

2. Data

The data in this study come from the South-western Ross Sea between February and November 2011. The measurements were transmitted from 16 CTD-SRDLs. The spatial and temporal distribution of the data are visualised in Fig. 1.

CTD-SRDLs measure conductivity, temperature, and depth (equivalent to pressure at approximately 1 m = 1 dbar). Previous laboratory testing (Böhme et al., 2009) showed that pressure measurements give errors of less than 1 dbar. Laboratory temperature readings are accurate, with a stated deviation of better than ± 0.005 °C and post-calibration checks giving averages of less than ± 0.002 °C. Errors in conductivity measurement have a stated accuracy of better than ± 0.005 °C and post-calibration deviations of better than ± 0.002 °C. This yields laboratory errors in salinity of ± 0.02 for the stated accuracies and ± 0.01 for the measured deviations. In situ errors from CTD-SRDLs deployed in parallel with standard shipboard CTDs were ± 0.03 °C and ± 0.01 for temperature and salinity, respectively (Roquet et al., 2009).

When deployed on marine mammals, CTD-SRDLs have been reported with errors of ± 0.02–0.03 °C and ± 0.03–0.05 psu *after correction* against historical deep measurements or the nearest contemporaneous Argo or ship data in waters around 65°S (Charrassin et al., 2008). In waters further north (mostly between 50 and 55°S), errors were reported by Roquet et al. (2011) as ± 0.02 °C and ± 0.1 psu before correction or ± 0.01 °C and ± 0.02 psu after correction based on comparison with similar data types.

Unlike this study, these data from CTD-SRDLs mounted on Elephant seals were at lower latitude, and with less or no ice cover. Goetz (2015) reported that, in combination with Weddell seal behaviour, sea ice influenced accuracy and resulted in more damage to hardware in comparison to CTD-SRDLs mounted on Elephant seals. In addition, for in situ results from CTD-SRDL tags deployed on Weddell seals in the Ross Sea, Goetz (2015) noted that mean absolute errors in temperature and conductivity based on the manufacturer's calibration and their independent calibration relative to a CTD profiler were both ~0.1 °C and ~0.3 mS cm^{-1}, compared to manufacturer stated accuracies of ± 0.005 °C and ± 0.01 mS cm^{-1}. This discrepancy between expected and actual errors in the Ross Sea surface waters suggests that CTD-SRDLs may experience sensor delay when actively sampling in a dynamic environment typical of these surface waters. By contrast, in the lab environment the sensors are permitted to come to equilibrium (Goetz, 2015). This is supported by findings of Roquet et al. (2011) who found larger errors using CTD-SRDLs in temperature and derived salinity when sampling rapid changes in temperature, suggested to be result of the core temperature of the tag affecting measurements. Hence, CTD-SRDLs deployed in sub-zero very cold waters at high latitude may be expected to experience errors greater than manufacturer-stated accuracies, and our aim is to improve the precision of in situ CTD-SRDL measurements in these hostile environments.

3. Methodology

3.1. Calibration

We used the TEOS-10 toolbox (IOC et al., 2010) for processing the oceanographic parameters. This newer oceanographic standard uses units of absolute salinity (g kg^{-1}) and conservative temperature (°C) in place of practical salinity (PSS-78) and potential temperature. Salinities (S) from this data set are absolute salinities. Near the surface, the difference between practical and absolute salinity can be quite significant (i.e. $S_A \sim 35 \mathrm{g kg}^{-1}$, $S_P \sim 34.8$) (Wright et al., 2011). We derived salinity values from conductivity measurements. The differences between potential and conservative temperature are small.

In order to improve the accuracy of our data set with post-deployment corrections, we compare CTD-SRDLs to investigate differences in salinity measurements. Assuming weak space-time variability of hydrological properties on the order of kilometres and days (Gordon et al., 2000), we considered measurement profiles from two separate CTD-SRDLs to be co-located if they occurred within defined time and space windows. We compared any measurements between CTD-SRDLs that were at the same depth, specifically using the fixed depths in each dive profile. Hence for co-located pairs, there were data at common depths from which we were able to estimate salinity measurement differences.

The fixed depths were those that the “broken stick” data compression algorithm of the CTD-SRDL always includes for satellite transmission (Fedak et al., 2002). This method of compression preserved important features in the dive profile. To ensure that the two co-incident measurements at the same depth were sufficiently similar, and to

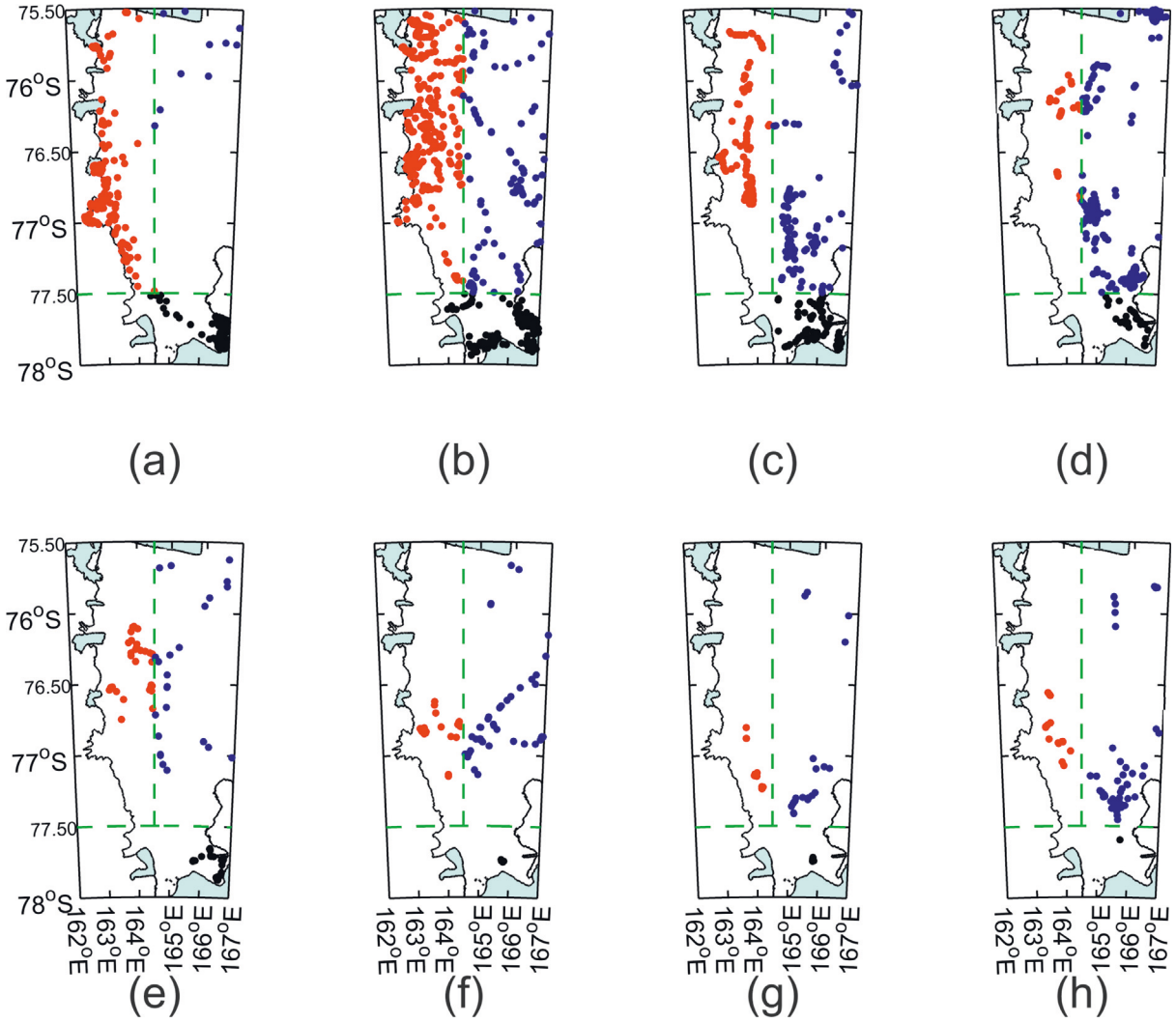

Fig. 1. Measurement profiles from February to September [(a)–(h)]. Each dot represents a vertical oceanographic profile. The green dashed lines separate the area into the three regions of interest (clockwise from top left): Victoria Land Coast (red); Non-Coastal Ross Sea (blue); McMurdo Sound (black). There is a diminishing sample size as the year progresses; see Discussion for details. (For interpretation of the references to colour in this figure legend, the reader is referred to the web version of this article.)

reduce variability driven by vertical motion in the water column, we also compared conservative temperature measurements from each depth pair. The measurements were rejected if this temperature difference was greater than $\Delta\Theta = 0.1$°C, the highest recorded mean absolute error of temperature from deployed CTD-SRDLs in Goetz (2015). Temperature differences greater that this difference were assumed to be due to measuring different water masses.

The limits in time and space that determine whether a pair of profiles is co-located were chosen such that they produced interactions between as many different CTD-SRDL pairs as possible without introducing unacceptably large error from space-time variations. Running trial co-locations with different limits allowed interpretation of the effect of limit choice on the number of co-located pairs. This is shown for the present data set in Fig. 2. The marked contour indicates the minimum limits required to produce as many equations in a linear system as there are salinity offset variables. In our system, this is equal to the number of CTD-SRDLs requiring correction, which is 16. Any choice below this would always produce an under-determined linear system. Any pair of limits that produces this many interactions or more will be sufficient. A suitable choice for this data set was 10 km and 2 days (Fig. 2), which provided a number of usable pairs well above the minimum required to avoid underdetermination. Note that in Fig. 2 only interactions with more than 30 co-incident measurements are counted.

Recalling that the temperatures (Θ) of co-located measurements are also required to be within 0.1 °C of each other, for a given pair of CTD-SRDLs, the mean salinity difference is the average difference in salinity measurements between all points at the same depth within 10 km and 2 days of each other, and satisfying $\Delta\Theta < 0.1$°C.

We included the measurements from the ITP as a known, high-quality reference to the CTD-SRDL data and performed the co-location process. The ITP makes high resolution measurements every 2 dbar, so it was possible to compare salinities at the appropriate CTD-SRDL fixed depths. Therefore, any CTD-SRDL that co-located at least once with the ITP could be directly compared to a known, accurate salinity. Salinity offsets were calculated based on these comparisons, so more co-locations between a CTD-SRDL and the ITP increased the confidence in our overall salinity offset correction. Note that not all CTD-SRDLs were co-located with the ITP in the present analysis. Had this been the case, direct comparisons between the ITP and CTD-SRDLs would have been possible.

Stated accuracies for measurements of temperature and conductivity for the Sea-Bird Electronics SBE-41 on the ITP are ± 0.002 °C and ± 0.002 mS cm^{-1}, and pressure is to within 2 dbar precision. The

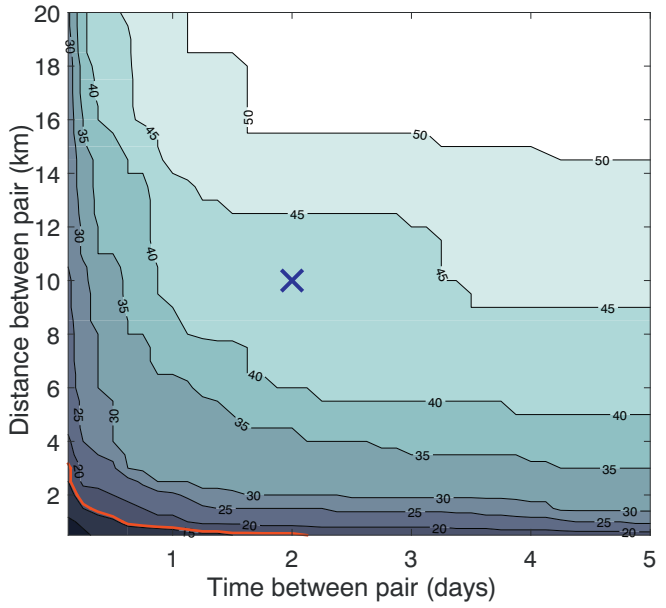

Fig. 2. Contour surface showing the number of pairs with more than 30 unique co-incident measurements. The contour of 16 pairs, the minimum required to avoid an under-determined system, is highlighted in red. The choice of limits to determine a co-located pair is indicated by the blue cross (at 2 days, 10 km). (For interpretation of the references to colour in this figure legend, the reader is referred to the web version of this article.)

manual states typical stabilities per year of 0.0002 °C for temperature and 0.0001 mS cm^{-1} for conductivity (with equivalent accuracy in salinity). Pressure stability was given as 0.8 dbar per year. The ITP was originally deployed at 77.8900 °S, 166.7905°E in late 2010 and remained at this position until it was dislodged by a large storm on 22 February 2011 (Hughes et al., 2014).

For a CTD-SRDL given by the index K, we have a set of salinity measurements S_K that, for each measurement, differ from the true salinity values $S_{K,0}$ by the single constant salinity offset for that CTD-SRDL, $\widetilde{S}_K$:

$$S_K - \widetilde{S}_K = S_{K,0}. \tag{1}$$

This salinity offset is unique to each CTD-SRDL; for the individual measurements i and j, from the two CTD-SRDLs K and L respectively,

$$\begin{aligned} S_{K,i} - \widetilde{S}_K &= S_{K,i,0}, \\ S_{L,j} - \widetilde{S}_L &= S_{L,j,0}, \end{aligned} \tag{2}$$

where we have indexed the individual salinity measurements ($S_{K,i}$ and $S_{L,j}$) to differentiate from the set of all measurements from that CTD-SRDL (S_K and S_L, respectively) and the salinity value at the point of each measurement is given by $S_{K,i,0}$ and $S_{L,j,0}$. We investigate the offsets by comparing pairs of measurements that are co-located. The co-location process finds all measurement profiles of K and L that are within 10 km and 2 days and compares the salinities at depths that are co-incident and satisfy $\Delta\Theta < 0.1$°C in each case. Using Eq. (1), for all n pairs of co-incident measurements between K and L,

$$(S_K - S_L) - (\widetilde{S}_K - \widetilde{S}_L) = S_{K,0} - S_{L,0}. \tag{3}$$

In theory, the RHS solution would be zero, given that the actual salinity value at two identical points in space and time are the same. However, our choice of co-locations here is imperfect in space and time, and small differences occur due to observation and measurement errors. We find the mean difference between the Kth and Lth CTD-SRDLs as follows:

$$A_{KL} = \frac{1}{n}\sum_{m=1}^{n}(S_{K,m} - S_{L,m}), \tag{4}$$

for each co-incident pair m. This allows us to rephrase Eq. (3) as

$$A_{KL} - (\widetilde{S}_K - \widetilde{S}_L) = \epsilon, \tag{5}$$

where ϵ is the residual, given by the difference between known, measured values (A_{KL}) and unknown, true values (which are here the actual salinity offsets $\widetilde{S}_K$, $\widetilde{S}_L$). Hence, the salinity offsets that best minimise the difference between measured values and expected values are given by minimising ϵ over CTD-SRDL pairs of K and L for all N CTD-SRDLs:

$$\chi^2 = \sum_{L=1}^{N}\sum_{K=1}^{L-1}\frac{(A_{KL} - (\widetilde{S}_K - \widetilde{S}_L))^2}{{\sigma_{KL}}^2}, \tag{6}$$

where we have divided by the variance of each average, as given by

$${\sigma_{KL}}^2 = \frac{1}{n}\sum_{m=1}^{n}((S_{k,m} - S_{l,m}) - A_{KL})^2. \tag{7}$$

We can rewrite some of these terms as matrices, and introduce the weighting matrix $\boldsymbol{W}$ as the inverse of the variances from Eq. (7), with which we will weight our final offset calculation to weight CTD-SRDL pairs with consistent differences in co-incident measurements:

$$\begin{aligned} \overrightarrow{A} &= \left[A_{21}, A_{31}, A_{32}, \ldots, 0\right] \\ \overrightarrow{S} &= \left[\widetilde{S}_1, \widetilde{S}_2, \ldots, \widetilde{S}_{ITP}\right] \\ \boldsymbol{W} &= \begin{pmatrix} \frac{1}{\sigma_{21}^2} & 0 & \ldots & 0 \\ 0 & \frac{1}{\sigma_{31}^2} & \ldots & 0 \\ \ldots & \ldots & \ldots & \ldots \\ 0 & 0 & \ldots & \sum\frac{1}{{\sigma_{KL}}^2} \end{pmatrix} \end{aligned} \tag{8}$$

where the ITP has been appended with zero measurement difference to actual salinity (i.e. such that $\widetilde{S}_{ITP} = 0$). Because it is an accurate instrument, we use the sum of all the other weights to ensure it is favourably considered by the system. This leads us to Eq. (6) and this is solvable as a matrix equation:

$$\chi^2 = \|\boldsymbol{W}(\overrightarrow{A} - \boldsymbol{D}\overrightarrow{S})\| \tag{9}$$

where $\boldsymbol{D}$ is the derivative matrix; i.e. it picks out values for $\widetilde{S}_K$ and $\widetilde{S}_L$ in each row as appropriate. The aim is to find $\overrightarrow{S}$ to best fit the equations. Hence, we find $\overrightarrow{S}$ such that:

$$\overrightarrow{S} = \arg\min_{\overrightarrow{S}}\chi^2(\overrightarrow{S}). \tag{10}$$

Since the N columns of $\mathbf{D}$ corresponding to the N CTD-SDRLs are linearly independent, we may solve the normal equations (Taylor, 1997)

$$(\mathbf{D}^T\mathbf{W}\mathbf{D})\overrightarrow{S} = \mathbf{D}^T\mathbf{W}\overrightarrow{A} \tag{11}$$

$$\overrightarrow{S} = (\mathbf{D}^T\mathbf{W}\mathbf{D})^{-1}\mathbf{D}^T\mathbf{W}\overrightarrow{A}. \tag{12}$$

The result of this calculation is a vector of offsets $\overrightarrow{S}$ where each $\widetilde{S}_K$ refers to the CTD-SRDL corresponding to K. These can be directly applied to the salinities S_K in order to return an approximation of the true set of salinities as in Eq. (1). To do this, we assume that these offsets are constant over the duration of the CTD-SRDL's deployment, and do not change with time or environmental factors.

3.2. Application

After correcting using such a technique, we investigated changes in the oceanographic structure of the South-western Ross Sea during 2011.

We organised our data into bins of 0.5 °C longitude by 0.25 °C latitude and 30 days. Profiles were then interpolated to measurements at 10 m intervals and averaged at these depths over each bin. This was necessary because the sampling was such that consecutive measurements were not taken at the same location nor the same time. Hence, we cannot compare observations across the entire region at a specific time, nor evolution over time at a particular location; however, by averaging, we obtained regional and monthly estimates of oceanographic parameters in order to identify overall trends in observations.

We demonstrate the utility of these derived regional changes in oceanographic structure over time by estimating the time evolution of sea ice thickness using corrected data. This is a suitable test case because it is only dependent on the changes in salinity with time, not the absolute value of salinity. Hence it allows us to evaluate whether we are successful in improving the precision of the salinity data without requiring exact knowledge of their accuracy. However, as can be seen in Fig. 1, there is a decline in available data in later months, which should be considered when interpreting results involving these data.

Within the defined spatial and temporal bins, we checked for cases of density inversion in the water column, which we considered to be when shallower water was denser by 0.05 g kg^{-1} than deeper water (Nguyen et al., 2009). This difference in density should result in immediate vertical mixing, so typically reflects an artefact of data processing in averaged data rather than a persistent feature. Therefore we removed any data showing such a density inversion. There were a further four profiles that showed clear signs of CTD-SRDL failure in their measurements, such as unphysically large vertical gradients. We removed these spurious measurements, and linearly interpolated the remaining data in these bins at 10 m intervals and averaged to get a "mean" profile for a given bin in a given month. This allowed us to track changes in oceanographic structure as a function of time and depth, within specific areas.

The change in the mass of salt present in the water is estimated by integrating the changes in salinity with time. As has been done previously (Charrassin et al., 2008; Leonard et al., 2011; Mahoney et al., 2011), we assume the increase in ocean salt content is due to salt rejection as a result of sea ice formation and thus the rate of ice growth. This process directly equates the change in salt mass within the column to the ice growth that would produce an equivalent change in salt mass, relying on the assumption that salinity changes in the water column are dominated by the growth of ice. In the South-western Ross Sea, lateral advection of high salinity water takes place from nearby Terra Nova Bay and Ross Sea polynyas (e.g. Manzella et al., 1999) where substantial ice growth occurs. This increases the uncertainty in our ice growth but does not prevent its calculation. In this paper, we follow a similar approach to these other studies as described to apply the corrected CTD-SRDL data to an investigation of ice growth due to changes in salinity.

Initially, we may find the total mass of salt per unit area of ocean by integrating salinity to a particular depth in the water column:

$$m_s(t) = \int_0^H \rho(z, t)S(z, t) \quad \mathrm{d}z, \tag{13}$$

or for the change in the mass of salt per unit area between times t_1 and t_2,

$$\Delta m_s = \int_0^H [\rho(z, t_1)S(z, t_1) - \rho(z, t_0)S(z, t_0)] \quad \mathrm{d}z \tag{14}$$

where H is the depth of integration, z is depth and t is time. In practice, we used our binned data, discretised at 10 m intervals, to estimate the integral. Further, we do not have a full description of the water column down to the ocean floor for the entire measuring period. Therefore, we chose a depth H for this upper layer that best described the change in the mass of salt as a result of brine rejection due to ice formation. In Charrassin et al. (2008), Leonard et al. (2011), and Mahoney et al. (2011), the thickness of sea ice formed is estimated for brine rejection that yields the observed changes in the mass of salt to depths of 100 m, 250 m, and 510 m, respectively. We investigate estimations of sea ice thickness using these values as our depth for the upper layer, H. This is based on the assumption that salt rejected by sea ice formation is retained almost entirely in this upper layer (Barthélemy et al., 2015). Hence, we consider any changes in salinity below the depth of H to be a result of other effects.

We related the change in salt mass to sea ice growth by calculating the amount of vertical growth, Δh, that would be responsible for the change in salt mass as calculated per unit area. We then compared these estimates to other measurements of sea ice thickness in the same timeframe and region (Price et al., 2014).

First we estimated the mass of salt displaced by the formation of ice of thickness Δh,

$$\Delta(m_s)_{displaced} = \Delta h\,[\rho_{surf}(t_0)S_{surf}(t_0) - \rho_{ice}S_{ice}]. \tag{15}$$

Note that $S_{ice} \approx 6\ \mathrm{g\,kg^{-1}}$ and $\rho_{ice} \approx 915\ \mathrm{kg\,m^{-3}}$ are approximations for the salinity (Gough et al., 2012) and density (Price et al., 2014) of sea ice in this part of the Ross Sea. ρ_{surf} and S_{surf} are the density and salinity respectively of the water at the surface that freezes in the ice formation process. Therefore, we used our shallowest measurements at $z_1 = 10$ m, to estimate these quantities such that $\rho_{surf}(t_0) = \rho(z_1,t_0)$ and $S_{surf} = S(z_1,t_0)$.

Equating the change in salt mass of Eq. (15) with the change in salt mass from Eq. (14) allowed us to solve for the change in sea ice thickness in metres:

$$\Delta h = \frac{\int_0^H [\rho(z, t_1)S(z, t_1) - \rho(z, t_0)S(z, t_0)] \quad \mathrm{d}z}{\rho(z_1, t_0)S(z_1, t_0) - \rho_{ice}S_{ice}}. \tag{16}$$

Eq. (16) is discretised to:

$$\Delta h = \frac{\sum_{a=1} [\rho_k(t_1)S_k(t_1) - \rho_k(t_0)S_k(t_0)]\Delta(z)}{\rho(z_1, t_0)S(z_1, t_0) - \rho_{ice}S_{ice}}, \tag{17}$$

for a discrete parameters beginning at a depth of $z_1 = 10$m down to the depth of $z_a = H$, where we have used $H = 100$m, 250m, and 510m as our depths for integration, and $\Delta z = 10$ m as the spacing between our discrete measurements.

We can estimate total sea ice thickness over time from these sea ice growth rates if we know when there was no ice cover. For this, we used the 22nd of February 2011 (Hughes et al., 2014), when a large storm broke up the remaining summer ice cover in the western Ross Sea, resulting in a nearly ice-free ocean. This is confirmed by the retreat of sea ice cover back to the ice shelf between MODIS satellite images taken on the 9th of February 2011 and the 24th of February 2011 (Scambos et al., 1996).

4. Results

4.1. Calibration

The effectiveness of the salinity correction method when applied to the study can be seen in Fig. 3, which shows the data before and after correction. In both, the data share similar distributions, but before correction (Fig. 3a) the data from each CTD-SRDL are shifted along the salinity axis with respect to other CTD-SRDLs.

Our estimates for the salinity corrections applied to individual CTD-SRDLs were of the order 10^{-1}gkg^{-1}, consistent with previous findings (e.g. Böhme et al., 2009). The improvement between measurements of salinity from pairs of co-located CTD-SRDLs is very significant. Post-correction, the absolute average differences in co-located salinity measurements between pairs of CTD-SRDLs show a decrease by a factor of 10 (Fig. 4).

A useful initial check that our corrected data behaves as we expect is provided in Fig. 5. Uncorrected winter data in Fig. 5a show a considerable spread in salinity. Following recalibration of the data so that

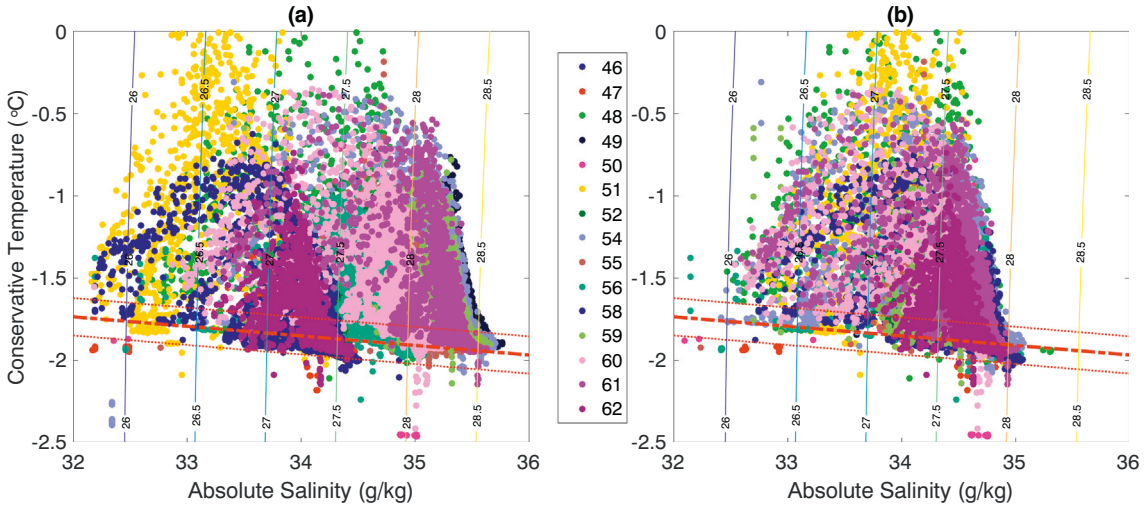

Fig. 3. All oceanographic data collected by CTD-SRDLs (a) pre- and (b) post- correction by the instrument-specific salinity offset. The red line indicates the freezing temperature of water at a given salinity. Density anomaly contours are also included. Each colour represents measurements made by a different CTD-SRDL, numbered by the last 2 digits of their unique identifiers. The prefix 1011 is omitted from the CTD-SRDL serial numbers for convenience. (For interpretation of the references to colour in this figure legend, the reader is referred to the web version of this article.)

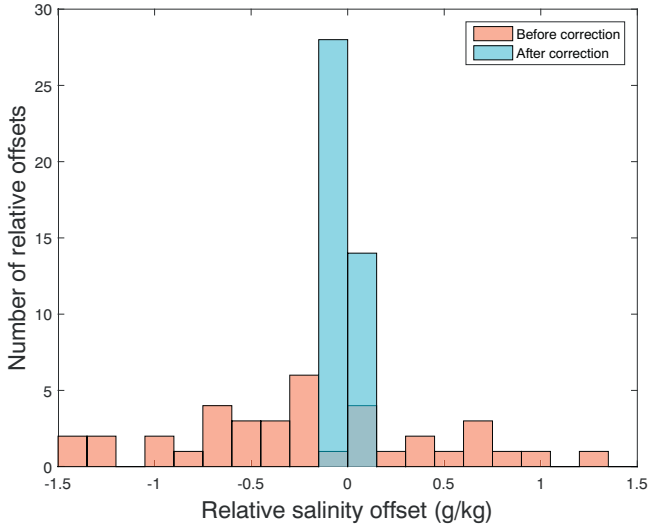

Fig. 4. Co-located salinity differences before (brown) and after (blue) correction. There is a decrease by an order of 10^{-1}gkg^{-1}. (For interpretation of the references to colour in this figure legend, the reader is referred to the web version of this article.)

salinity offsets are accounted for, Fig. 5b shows the data in agreement with each other and with the expectation that water will be at the freezing temperature in winter, within the uncertainty associated with the correction method. This is taken to be the maximum mean absolute error of measurements between devices post-calibration, $\sim 0.14\,\mathrm{g\,kg^{-1}}$ (see Fig. 4).

4.2. Application

Using the binned data, we are able to track and visualise changes in oceanographic parameters as seen in Fig. 6, where the bins are further averaged over McMurdo Sound, Victoria Land Coast, and the Non-Coastal Ross Sea. The boundaries for these regions of interest are shown in Fig. 1.

To create regional approximations of sea ice thickness over time in the three areas indicated in Fig. 1, the estimated ice growth is calculated for each bin where sufficient data are available and then averaged over each region and presented as ice thickness in Fig. 7 alongside direct drill hole sea ice thickness measurements from within the McMurdo Sound region in November 2011 (Price et al., 2014). The spread in these direct measurements represents the spatial variation due to measurements being made across the fast ice of McMurdo Sound. Estimated ice thickness is shown for three different values of H, the depth to which salinity changes over time are assumed to be a product of ice formation in this prediction.

5. Discussion

The method presented here for correcting for the salinity offset of these CTD-SRDLs reduces the discrepancy between CTD-SRDL measurements by a factor of 10 for the data used in this study from discrepancies as large as $1.42\,\mathrm{g\,kg^{-1}}$ to $\leq 0.14\,\mathrm{g\,kg^{-1}}$.

Therefore, by applying an instrument-specific offset to all measurements of salinity, we have improved the calibration. Temperature-salinity plots before and after accounting for instrument-specific offsets are shown in Fig. 3. We also present data from winter only (July–November 2011) in Fig. 5. In Figs. 3 and 5, the red freezing line indicates the temperature at which a parcel of water of given salinity will freeze if moved to surface pressure. In winter, sea ice formation drives the production of high salinity water at the freezing temperature at the surface of the water. Vertical mixing due to the cold, high salinity (high density) water drives the cooling of the upper water column to freezing temperature. Therefore, we should expect all data to sit close to the line of freezing temperature during winter. However, interaction with a nearby ice shelf at depth may cause supercooling (e.g. Leonard et al., 2011). One example of interest is the small collection of points below our estimated error for the freezing temperature (Fig. 5), CTD-SRDL 101160. These measurements were taken in September off the Victoria Land coast at co-ordinates of approximately 77 °S, 164 °E. From the location, these measurement plausibly originate from the 35 km wide supercooled Ice Shelf Water plume that exits from the Western McMurdo Ice Shelf and travels northward (Robinson et al., 2014). Thus the position of the corrected data on T-S diagrams in winter months meets expectations for the behaviour of sea water beneath sea ice, providing confidence that co-locations including the accurate oceanographic instrument produces a suitable correction.

When a reference instrument is not used alongside CTD-SRDL data, the absolute accuracy of the salinity is unknown. However, changes in salinity can still be accurately observed when corrected for instrument-

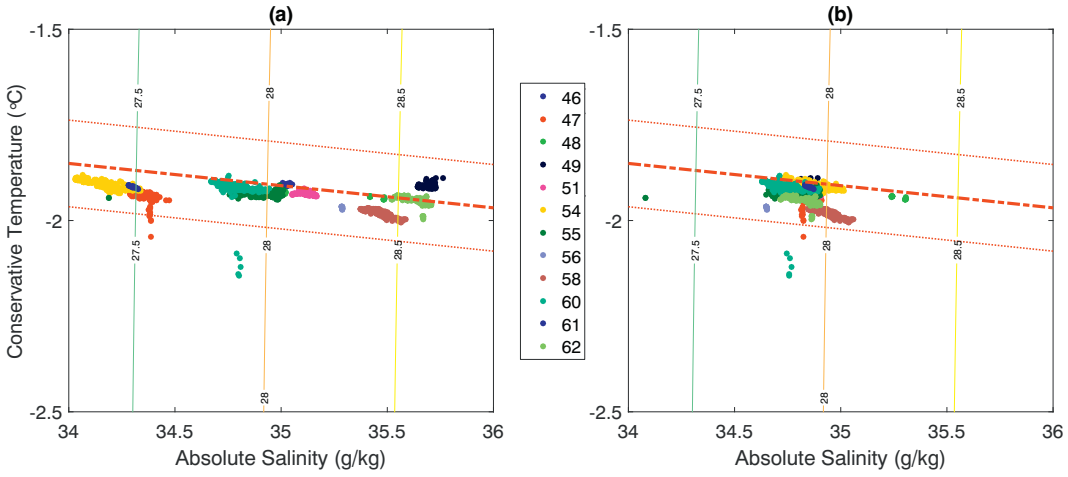

Fig. 5. Data from complete profiles between July and November 2011 (inclusive) pre- (a) and post- (b) correction by the instrument-specific salinity offset. Error bounds on the freezing temperature are shown as thinner red lines above and below the dashed red freezing line for sea water. Salinity errors are derived from the maximum mean absolute error of measurements between devices post-calibration, $\sim 0.14\,\mathrm{g\,kg^{-1}}$. The error bars for temperature are from Goetz (2015), where the highest recorded mean absolute error of temperature from deployed devices was $\sim 0.1\,^{\circ}\mathrm{C}$. Colours represent measurements made by different CTD-SRDLs. (For interpretation of the references to colour in this figure legend, the reader is referred to the web version of this article.)

dependent offset. Because sea ice thickness estimation in this way requires only these changes and not the absolute value of salinity, it is an application that can be used without requirement for a reference instrument.

Within the regional sea ice thickness estimations, the use of an integration depth of $H = 100\,\mathrm{m}$ (Charrassin et al., 2008) produced an estimate for regional sea ice thickness within the spread of direct measurements from the same region in Price et al. (2014). This approximate agreement suggests that using salinity changes to an appropriate layer depth as a proxy to sea ice growth produces reasonable estimates of sea ice thickness in regions where direct measurements are not available. We can further note that the CTD-SRDL data in the McMurdo Sound region come primarily from the east side, near Ross Island, an area where Price et al. (2014) found lower ice thicknesses. This is of interest because we see that in Fig. 7, our McMurdo Sound ice thickness is projected to be slightly less than the average ice thickness in Price et al. (2014).

However, we found that integrations to depths of 250 m and 510 m yielded larger sea ice thickness estimates. This was an expected result, consistent with other studies (Leonard et al., 2011; Mahoney et al., 2011). In Leonard et al. (2011), data obtained from conventional CTD casts down to 250 m gave salinity changes that suggested ice growth was a factor of approximately two greater than drill hole measurements. In Mahoney et al. (2011), a similar conclusion was reached for salinity changes down to 510 m. In this study, we do observe that the deeper two values for H produce approximately twice the ice thickness than that found for the shallower H. We suggest then that in this study most of the salinity change in the water column pertaining to rejection during sea ice formation is retained in the upper water column to approximately 100 m, and that salinity changes beneath this depth are a result of high salinity water being imported from elsewhere. Leonard et al. (2011) and Mahoney et al. (2011) both attributed the excess salt in McMurdo Sound as arising from lateral advection from Ross Sea and Terra Nova Bay Polynyas, both of which are areas of high sea ice production and hence producers of high salinity water.

Precipitation, evaporation, and other related processes are assumed to be minimal in the measurements made in comparison to salinity changes due to sea ice formation or lateral advection in this study. In other studies (e.g. Charrassin et al., 2008), it is suggested that freshening due to net precipitation yields the biggest error contribution, $< 0.3\,\mathrm{cm\,d^{-1}}$, which leads to underestimation of sea ice formation rates. However, comparison to direct ice thickness measurements in this study suggests overestimation of sea ice formation rates. In the context of the region of this study, we have a strong source of lateral advection of high salinity water from polynyas, and for most of the season we are in regions of very high ice concentrations due to sustained growth of ice and proximity to ice shelves which in turn impedes direct ocean-atmosphere interactions. Therefore, other freshening process are likely to be small in comparison, and the majority of the detected change in salinity that is not due to ice formation can likely be attributed to lateral advection.

It is not possible to accurately and independently quantify all of the errors arising from sources of salinity other than ice formation. However, we are able to comment on the statistical error associated with the diminishing sample size in each region as the season progresses (Figs. 1, 8). This considers error arising purely from small sample sizes, not systematic errors, giving us a lower bound for the overall error including systematic errors (e.g. from assuming no lateral advection) and highlights the issue of diminishing transmission rates from the CTD-SRDLs. Standard errors ($\sigma_{\bar{x}}$) of the mean prediction for ice growth rates are shown out to $\pm\, 1\sigma_{\bar{x}}$ ($\pm$ 34%) in Fig. 8 along with the associated sample size for that estimate, and is calculated from the sample standard deviation. It is clear that sampling by CTD-SRDLs is not always random, which is expected given that the seals will tend to follow resources such as food and breathing holes, and thus swap between selectively sampling specific locations. Further, statistical errors proportional to the estimate are inversely proportional to the sample size as is expected. For very small N, this can cause $\sigma_{\bar{x}}$ to be almost as wide as the estimate of the mean itself. This causes greater uncertainty in mean ice growth estimates later in the season as the sample size diminishes.

6. Conclusion

In this paper, we have developed a method that improves the offset of data transmitted by CTD-SRDLs by a factor of 10. That is, variations of approximately $1.5\,\mathrm{g\,kg^{-1}}$ between co-located sensors were reduced to $0.15\,\mathrm{g\,kg^{-1}}$. By co-locating the CTD-SRDL data with an accurate reference instrument, we have also been able to improve confidence in the salinity accuracy.

Estimates of sea ice thickness do not require an accurate salinity data set, only that the data set is self-consistent and sufficiently precise. Our correction method, which emphasises the reduction of the absolute difference in co-located salinity measurements between CTD-SRDLs, produces such a data set. Using this, we are able to apply the CTD-SRDL

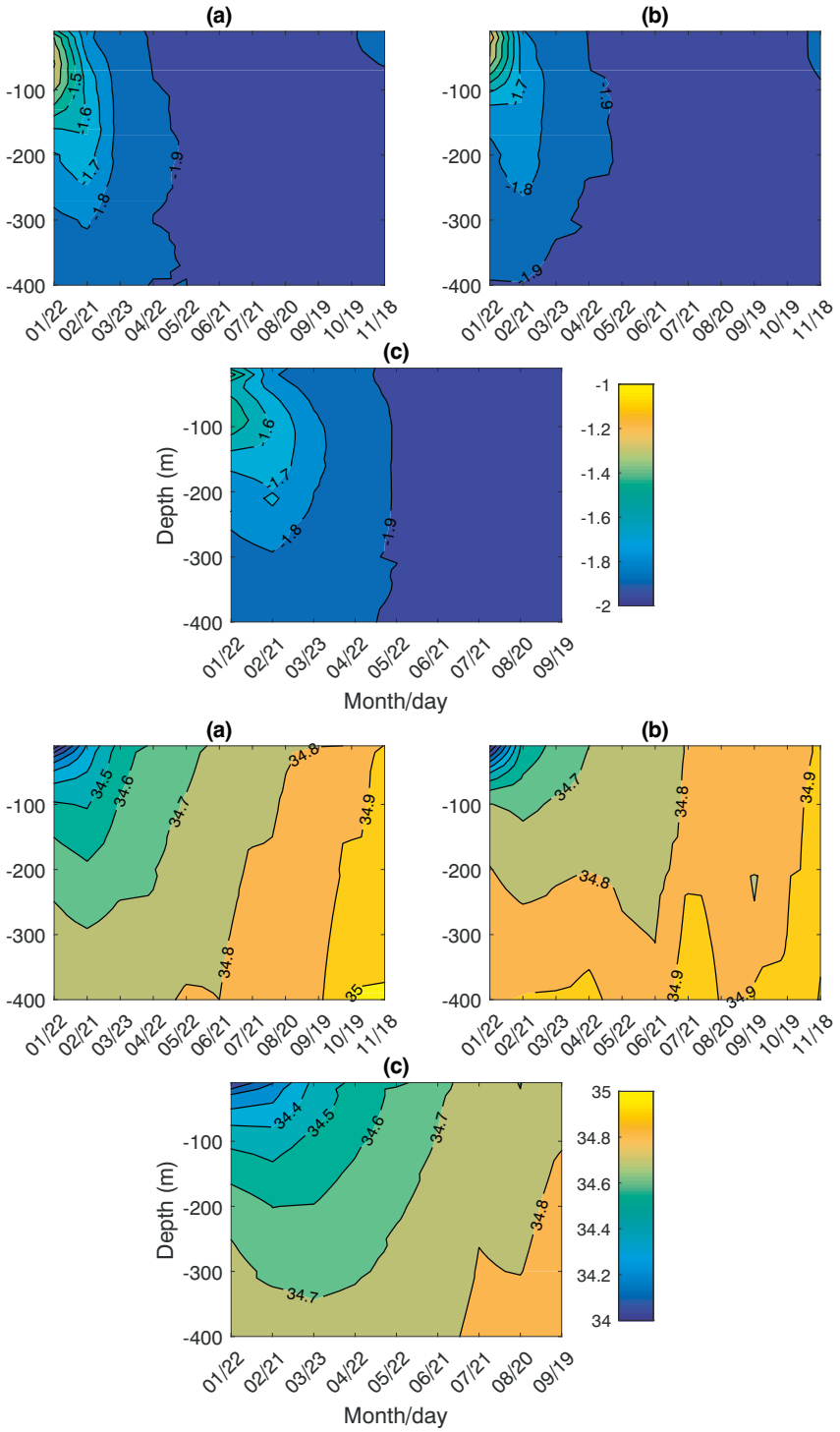

Fig. 6. Time series of oceanographic structure at depth. Figures shown are salinity in (a) Victoria Land Coast, (b) Non-Coastal Ross Sea, and (c) McMurdo Sound and temperature in (d) Victoria Land Coast, (e) Non-Coastal Ross Sea, and (f) McMurdo Sound. These regions are shown in Fig. 1.

data to the prediction of regional sea ice thickness, and to compare different depths to which sea ice formation affects salinity. We compare these results with direct sea ice measurements from the same time and area and verify that we are able to produce similar estimates using one of these depths.

The quality of the oceanographic data collected by CTD-SRDLs in this study suggests they may be limited when deployed on marine animals and at low temperatures, preventing them from being a complete replacement for other measurement platforms. However, the usefulness of oceanographic data with wide spatial and temporal extent is clear, and CTD-SRDLs are capable of collecting oceanographic data in areas that are typically inaccessible by other technologies, providing superior data coverage than would otherwise be available.

Acknowledgments

The authors are grateful to the University of Otago, theNIWA core funded project, Antarctic and High Latitude Climate, and the Deep South National Challenge, for financial support for this project. The authors are also grateful to Jennifer M. Burns, from the University of

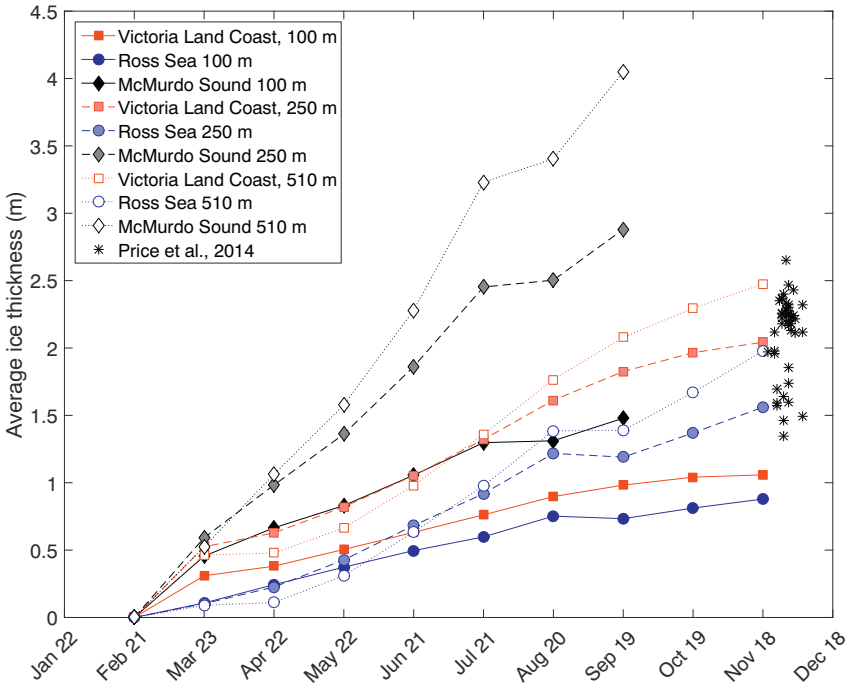

Fig. 7. Ice thicknesses from each region averaged over each temporal bin alongside direct measurements from across the McMurdo Sound region from Price et al. (2014), displayed as black asterisks. Solid, dashed, and dotted lines correspond to integration down to $H = 100$ m, 250 m, and 510 m respectively. Black diamonds, red squares, and blue circles correspond to the McMurdo Sound, Victoria Land Coast, and the Non-Coastal Ross Sea regions, respectively. (For interpretation of the references to colour in this figure legend, the reader is referred to the web version of this article.)

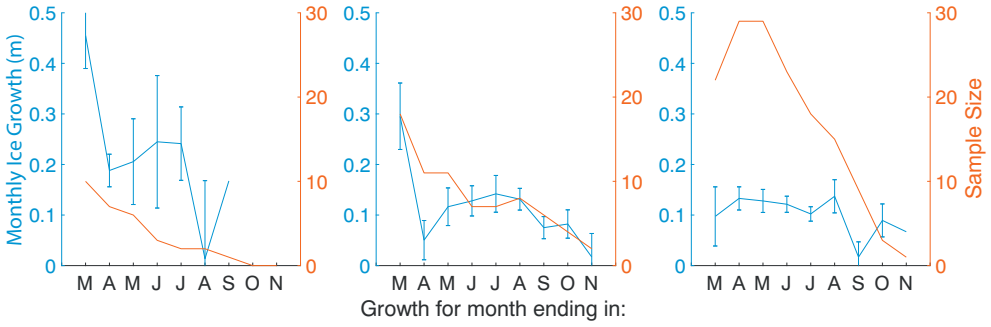

Fig. 8. Monthly ice growth rates separated into the three regions. From left to right: McMurdo Sound, Victoria Land Coast, and Non-Coastal Ross Sea. Standard errors for the estimation of the mean ice growth are shown as error bars for each estimate, and the sample size for each estimation of ice growth is overlaid. The statistical standard error proportional to the estimate is clearly inversely proportional to the sample size as expected.

Alaska Anchorage, who was co-principal investigator on the grant that funded all of the field work, and Alena Malyarenko, from the University of Otago, who contributed data processing advice and provided insight to expected oceanography.

The CTD-SRDL deployments were supported by the National Science Foundation (NSF) Office of Polar Programs (ANT-0838892) and L. Hückstädt, L. Pearson, J. Maresh, M. LaRue, B. Herried, P. Robinson, C. Burns, M. Zavanelli, and A. Eilers assisted in their deployment.

The St Andrews Sea Mammal Research Unit are also acknowledged for their ongoing commitment to developing and improving marine mammal oceanographic measurement platforms.

References

Aoki, S., Rintoul, S.R., Ushio, S., Watanabe, S., Bindoff, N.L., 2005. Freshening of the Adélie Land Bottom water near 140 E. Geophys. Res. Lett. 32 (23).

Barthélemy, A., Fichefet, T., Goosse, H., Madec, G., 2015. Modeling the interplay between sea ice formation and the oceanic mixed layer: limitations of simple brine rejection parameterizations. Ocean Model. 86, 141–152 Feb.

Böhme, L., Lovell, P., Biuw, M., Roquet, F., Nicholson, J., Thorpe, S.E., Meredith, M.P., Fedak, M., 2009. Technical note: animal-borne CTD-Satellite Relay Data Loggers for real-time oceanographic data collection. Ocean Sci. 5 (4), 685–695 Dec.

Böhme, L., Send, U., 2005. Objective analyses of hydrographic data for referencing profiling float salinities in highly variable environments. Deep Sea Research Part II: Topical Studies in Oceanography 52 (3-4), 651–664 Feb.

Charrassin, J.-B., Hindell, M., Rintoul, S., Roquet, F., Sokolov, S., Biuw, M., Costa, D., Boehme, L., Lovell, P., Coleman, R., et al., 2008. Southern Ocean frontal structure and sea-ice formation rates revealed by elephant seals. Proc. Natl. Acad. Sci. 105 (33), 11634–11639 Aug.

Costa, D.P., Klinck, J.M., Hofmann, E.E., Dinniman, M.S., Burns, J.M., 2008. Upper ocean variability in west Antarctic Peninsula continental shelf waters as measured using instrumented seals. Deep-Sea Res. II Top. Stud. Oceanogr. 55 (3-4), 323–337 Feb.

Durand, F., Reverdin, G., 2005. A statistical method for correcting salinity observations from autonomous profiling floats: an ARGO perspective. J. Atmos. Ocean. Technol. 22 (3), 292–301 Mar.

Fedak, M., 2004. Marine animals as platforms for oceanographic sampling: a "win/win" situation for biology and operational oceanography. Mem. Natl. Inst. Polar Res. Spec. Issue Jpn. 58, 133–147.

Fedak, M., Lovell, P., McConnell, B., Hunter, C., 2002. Overcoming the constraints of long range radio telemetry from animals: getting more useful data from smaller packages. Integr. Comp. Biol. 42 (1), 3–10 Feb.

Gille, S.T., 2002. Warming of the Southern Ocean since the 1950s. Science 295 (5558), 1275–1277 Feb.

Goetz, K.T., 2015. Movement, Habitat, and Foraging Behavior of Weddell Seals (*Leptonychotes weddellii*) in the Western Ross Sea, Antarctica. Ph.D. thesis. University of California Santa Cruz.

Gordon, C., Cooper, C., Senior, C.A., Banks, H., Gregory, J.M., Johns, T.C., Mitchell, J.F.B., Wood, R.A., 2000. The simulation of SST, sea ice extents and ocean heat transports in a version of the Hadley Centre coupled model without flux adjustments. Clim. Dyn. 16 (2-3), 147–168 Feb.

Gough, A., Mahoney, A., Langhorne, P., Williams, M., Haskell, T., 2012. Sea ice salinity and structure: a winter time series of salinity and its distribution. J. Geophys. Res. Oceans 117 (C3) Mar.

Hughes, K.G., Langhorne, P.J., Leonard, G.H., Stevens, C.L., 2014. Extension of an ice shelf water plume model beneath sea ice with application in McMurdo Sound, Antarctica. J. Geophys. Res. Oceans 119 (12), 8662–8687 Dec.

IOC, SCOR, IAPSO, 2010. The international thermodynamic equation of seawater — 2010: calculation and use of thermodynamic properties. In: Intergovernmental Oceanographic Commission, Manuals and Guides No. 56 (56), pp. 196 pp.

Jacobs, S., Giulivi, C., Mele, P., 2002. Freshening of the Ross Sea during the late 20th century. Science 297 (5580), 386–389 Jul.

Krishfield, R., Toole, J., Proshutinsky, A., Timmermans, M.-L., 2008. Automated ice-

tethered profilers for seawater observations under pack ice in all seasons. J. Atmos. Ocean. Technol. 25 (11), 2091–2105 Nov.
Kurtz, N.T., Markus, T., 2012. Satellite observations of Antarctic sea ice thickness and volume. J. Geophys. Res. Oceans 117 (C8) Aug.
Leonard, G.H., Langhorne, P.J., Williams, M.J., Vennell, R., Purdie, C.R., Dempsey, D.E., Haskell, T.G., Frew, R.D., 2011. Evolution of supercooling under coastal Antarctic sea ice during winter. Antarct. Sci. 23 (04), 399–409 apr.
Levitus, S., Antonov, J.I., Boyer, T.P., Stephens, C., 2000. Warming of the world ocean. Science 287 (5461), 2225–2229 Mar.
Mahoney, A.R., Gough, A.J., Langhorne, P.J., Robinson, N.J., Stevens, C.L., Williams, M.M.J., Haskell, T.G., 2011. The seasonal appearance of ice shelf water in coastal Antarctica and its effect on sea ice growth. J. Geophys. Res. Oceans 116 (C11), C11032 Nov.
Manzella, G.M.R., Meloni, R., Picco, P., 1999. Current, Temperature and Salinity Observations in the Terra Nova Bay Polynya Area. In: Oceanography of the Ross Sea Antarctica. Springer Milan, pp. 165–173.
Massom, R.A., Eicken, H., Hass, C., Jeffries, M.O., Drinkwater, M.R., Sturm, M., Worby, A.P., Wu, X., Lytle, V.I., Ushio, S., Morris, K., Reid, P.A., Warren, S.G., Allison, I., 2001. Snow on Antarctic sea ice. Rev. Geophys. 39 (3), 413–445 Aug.
Meredith, M.P., Ducklow, H.W., Schofield, O., Wåhlin, A., Newman, L., Lee, S., 2016. The interdisciplinary marine system of the Amundsen Sea, Southern Ocean: recent advances and the need for sustained observations. Deep-Sea Res. II Top. Stud. Oceanogr. 123, 1–6 Jan.
Meredith, M.P., Nicholls, K.W., Renfrew, I.A., Boehme, L., Biuw, M., Fedak, M., 2011. Seasonal evolution of the upper-ocean adjacent to the South Orkney Islands, Southern Ocean: results from a “lazy biological mooring”. Deep-Sea Res. II Top. Stud. Oceanogr. 58 (13-16), 1569–1579 Jul.
Meredith, M.P., Schofield, O., Newman, L., Urban, E., Sparrow, M., 2013. The vision for a Southern Ocean observing system. Curr. Opin. Environ. Sustain. 5 (3), 306–313 Sep.
Nguyen, A.T., Menemenlis, D., Kwok, R., 2009. Improved modeling of the Arctic halocline with a subgrid-scale brine rejection parameterization. J. Geophys. Res. Oceans 114 (C11), C11014 Nov.
Ozsoy-Cicek, B., Ackley, S., Xie, H., Yi, D., Zwally, J., 2013. Sea ice thickness retrieval algorithms based on in situ surface elevation and thickness values for application to altimetry. J. Geophys. Res. Oceans 118 (8), 3807–3822 Aug.
Pellichero, V., Sallée, J.-B., Schmidtko, S., Roquet, F., Charrassin, J.-B., 2017. The ocean mixed layer under Southern Ocean sea-ice: seasonal cycle and forcing. J. Geophys. Res. Oceans 122 (2), 1608–1633 Feb.
Price, D., Beckers, J., Ricker, R., Kurtz, N., Rack, W., Haas, C., Helm, V., Hendricks, S., Leonard, G., Langhorne, P., 2015. Evaluation of CryoSat-2 derived sea-ice freeboard over fast ice in McMurdo Sound, Antarctica. J. Glaciol. 61 (226), 285–300 May.
Price, D., Rack, W., Haas, C., Langhorne, P.J., Marsh, O., 2013. Sea ice freeboard in McMurdo Sound, Antarctica, derived by surface-validated ICESat laser altimeter data. J. Geophys. Res. Oceans 118 (7), 3634–3650 Jul.
Price, D., Rack, W., Langhorne, P., Haas, C., Leonard, G., Barnsdale, K., 2014. The sub-ice platelet layer and its influence on freeboard to thickness conversion of Antarctic sea ice. Cryosphere 8 (3), 1031–1039 Jun.
Robinson, N.J., Williams, M.J.M., Stevens, C.L., Langhorne, P.J., Haskell, T.G., 2014. Evolution of a supercooled Ice Shelf Water plume with an actively growing subice platelet matrix. J. Geophys. Res. Oceans 119 (6), 3425–3446 Jun.
Roquet, F., Charrassin, J.-B., Marchand, S., Boehme, L., Fedak, M., Reverdin, G., Guinet, C., 2011. Delayed-mode calibration of hydrographic data obtained from animal-borne satellite relay data loggers. J. Atmos. Ocean. Technol. 28 (6), 787–801 Jun.
Roquet, F., Park, Y.-H., Guinet, C., Bailleul, F., Charrassin, J.-B., 2009. Observations of the Fawn Trough Current over the Kerguelen Plateau from instrumented elephant seals. J. Mar. Syst. 78 (3), 377–393 Oct.
Roquet, F., Wunsch, C., Forget, G., Heimbach, P., Guinet, C., Reverdin, G., Charrassin, J.-B., Bailleul, F., Costa, D.P., Huckstadt, L.A., Goetz, K.T., Kovacs, K.M., Lydersen, C., Biuw, M., Nøst, O.A., Bornemann, H., Ploetz, J., Bester, M.N., McIntyre, T., Muelbert, M.C., Hindell, M.A., McMahon, C.R., Williams, G., Harcourt, R., Field, I.C., Chafik, L., Nicholls, K.W., Boehme, L., Fedak, M.A., 2013. Estimates of the Southern Ocean general circulation improved by animal-borne instruments. Geophys. Res. Lett. 40 (23) Dec. 2013GL058304.
Scambos, T., Bohlander, J., Raup, B., 1996. Images of Antarctic Ice Shelves (February 2011).
Electronics, Sea-Bird, 2014. SBE 41/41CP CTD Module for Autonomous Profiling Floats (Argo). http://www.seabird.com/sbe41-argo-ctd.
Smith, W., Goetz, K., Kaufman, D., Queste, B., Asper, V., Costa, D.P., Dinniman, M.S., Friedrichs, M.A., Hofmann, E.E., Heywood, K.J., et al., 2014. Multiplatform, multidisciplinary investigations of the impacts of modified Circumpolar Deep Water in the Ross Sea, Antarctica. Oceanography 2 (2) Jun.
St Andrews Sea Mammal Research Unit, 2003. SMRU CTD-SRDL Instrumentation. [Online; last accessed 16-December-2018],
Taylor, J.R., 1997. Introduction to Error Analysis: The Study of Uncertainties in Physical Measurements. University Science Books.
Treasure, A., Roquet, F., Ansorge, I., Bester, M., Boehme, L., Bornemann, H., Charrassin, J.-B., Chevallier, D., Costa, D., Fedak, M., Guinet, C., Hammill, M., Harcourt, R., Hindell, M., Kovacs, K., Lea, M.-A., Lovell, P., Lowther, A., Lydersen, C., McIntyre, T., McMahon, C., Muelbert, M., Nicholls, K., Picard, B., Reverdin, G., Trites, A., Williams, G., de Bruyn, P.N., 2017. Marine mammals exploring the oceans pole to pole: a review of the MEOP consortium. Oceanography 30 (2), 132–138 Jun.
Wright, D., Pawlowicz, R., McDougall, T., Feistel, R., Marion, G., 2011. Absolute Salinity, “Density Salinity” and the Reference-Composition Salinity Scale: present and future use in the seawater standard TEOS-10. Ocean Sci. 7 (1), 1–26 Jan.
Xie, H., Tekeli, A.E., Ackley, S.F., Yi, D., Zwally, H.J., 2013. Sea ice thickness estimations from ICESat altimetry over the Bellingshausen and Amundsen Seas, 2003-2009. J. Geophys. Res. Oceans 118 (5), 2438–2453 May.
Zwally, H.J., Yi, D., Kwok, R., Zhao, Y., 2008. ICESat measurements of sea ice freeboard and estimates of sea ice thickness in the Weddell Sea. J. Geophys. Res. Oceans 113 (C2), C02S15 Feb.